ACADEMIC PRESS

Available online at www.sciencedirect.com

SCIENCE DIRECT®

Journal of Computational Physics 187 (2003) 318–342

JOURNAL OF COMPUTATIONAL PHYSICS

www.elsevier.com/locate/jcp

Numerical solution of the Gross–Pitaevskii equation for Bose–Einstein condensation

Weizhu Bao [a,*], Dieter Jaksch [b], Peter A. Markowich [c]

[a] *Department of Computational Science, National University of Singapore, Singapore 117543, Singapore*
[b] *Institut für Theoretische Physik, Universität Innsbruck, Innsbruck A-6020, Austria*
[c] *Institute of Mathematics, University of Vienna, Boltzmanngasse 9, Vienna A-1090, Austria*

Received 8 February 2002; received in revised form 17 February 2003; accepted 17 February 2003

Abstract

We study the numerical solution of the time-dependent Gross–Pitaevskii equation (GPE) describing a Bose–Einstein condensate (BEC) at zero or very low temperature. In preparation for the numerics we scale the 3d Gross–Pitaevskii equation and obtain a four-parameter model. Identifying 'extreme parameter regimes', the model is accessible to analytical perturbation theory, which justifies formal procedures well known in the physical literature: reduction to 2d and 1d GPEs, approximation of ground state solutions of the GPE and geometrical optics approximations. Then we use a time-splitting spectral method to discretize the time-dependent GPE. Again, perturbation theory is used to understand the discretization scheme and to choose the spatial/temporal grid in dependence of the perturbation parameter. Extensive numerical examples in 1d, 2d and 3d for weak/strong interactions, defocusing/focusing nonlinearity, and zero/nonzero initial phase data are presented to demonstrate the power of the numerical method and to discuss the physics of Bose–Einstein condensation.

Keywords: Bose–Einstein condensation (BEC); Gross–Pitaevskii equation; Time-splitting spectral method; Approximate ground state solution; Defocusing/focusing nonlinearity

1. Introduction

Recent experimental advances in achieving and observing Bose–Einstein condensation (BEC) in trapped neutral atomic vapors [5,11,20] have spurred great excitement in the atomic physics community and renewed the interest in studying the collective dynamics of macroscopic ensembles of atoms occupying the same one-particle quantum state [19,30,42]. The condensate typically consists of a few thousands to

* Corresponding author. Tel.: +65-6874-3337; fax: +65-6774-6756.
E-mail addresses: bao@cz3.nus.edu.sg (W. Bao), d.jaksch1@physics.ox.ac.uk (D. Jaksch), peter.markowich@univie.ac.at (P.A. Markowich).
URL: http://mailbox.univie.ac.at/peter.markowich.

0021-9991/03/$ - see front matter
doi:10.1016/S0021-9991(03)00102-5

millions of atoms which are confined by a trap potential. In fact, beside the effects of the internal interactions between the atoms, the macroscopic behavior of BEC matter is highly sensitive to the shape of this external trapping potential. Theoretical predictions of the properties of a BEC like the density profile [10], collective excitations [23] and the formation of vortices [46] can now be compared with experimental data [5,33,41]. Needless to say that this dramatic progress on the experimental front has stimulated a wave of activity on both the theoretical and the numerical front.

The properties of a BEC at temperatures T much smaller than the critical condensation temperature T_c [35] are usually well modeled by a nonlinear Schrödinger equation (NLSE) for the macroscopic wave function [30,35] known as the Gross–Pitaevskii equation (GPE) [31,44], which incorporates the trap potential as well as the interactions among the atoms. The effect of the interactions is described by a mean field which leads to a nonlinear term in the GPE. The cases of repulsive and attractive interactions – which can both be realized in the experiment – correspond to defocusing and focusing nonlinearities in the GPE, respectively. Note that equations very similar to the GPE also appear in nonlinear optics where an index of refraction, which depends on the light intensity, leads to a nonlinear term like the one encountered in the GPE.

There has been a series of recent studies which deals with the numerical solution of the time-independent GPE for the ground state and the time-dependent GPE for finding the dynamics of a BEC. Bao and Tang [8] presented a general method to compute the ground state solution via directly minimizing the energy functional and used it to compute the ground state of the GPE in different cases. Edwards and Burnett [24] introduced a Runge–Kutta type method and employed it to solve the spherically symmetric time-independent GPE. Adhikari [1,2] used this approach to obtain the ground state solution of the GPE in 2d with radial symmetry. Other approaches include a finite difference method proposed by Chiofalo et al. [17] and Schneider et al. [49] and a simple analytical method proposed by Dodd [21]. For the numerical solution of the time-dependent GPE only few methods are available, a particle-inspired scheme proposed by Cerimele et al. [15,16] and a finite difference method used by Ruprecht et al. [47] and Ensher et al. [25].

In this paper, we take the 3d Gross–Pitaevskii equation, make it dimensionless to obtain a four-parameter model, use (singular) perturbation theory to discuss semiclassical asymptotics, to approximately reduce it to a 2d GPE and a 1d GPE in certain limits, and discuss the approximate ground state solution of the GPE in two extreme regimes: (very) weak interactions and strong repulsive interactions, again using perturbation methods. Numerical computations for similar physical set ups can to a large extent be found in the physical literatures cf. [10], however they are included here since perturbation theory gives a systematic way to obtain rigorously (validate) these approximations and since they are used as important preparatory steps for the numerical simulations (approximate ground states usually serve as initial data). Then we use the time-splitting spectral method, which was studied in Bao et al. [6,7] for the Schrödinger equation in the semiclassical regime, to discretize the time-dependent GPE. The merit of the numerical method is that it is explicit, unconditionally stable, time reversible, time-transverse invariant, and conserves the position density. In fact, the spectral method has shown great success in solving problems arising from many areas of science [12,29] due to its spatially spectral accuracy. The split-step procedure was presented for differential equations in [50] and applied to Schrödinger equations [26,32,51] and the KdV equation [52], as well as used with an iterative procedure for optical fibers [4]. In this paper we perform grid control using singular perturbation theory and present extensive numerical examples in 1d, 2d and 3d for weak/strong interactions, defocusing/focusing nonlinearity, and zero/nonzero initial phase data.

The paper is organized as follows. In Section 2 we start out with the 3d GPE, scale it to get a four-parameter model, show how to reduce it to lower dimensions and give the approximate ground state solution in the two mentioned extreme regimes of (very) weak interactions and strong repulsive interactions and discuss semiclassical asymptotics. In Section 3 we present the time-splitting spectral method for the GPE. In Section 4 numerical tests of the GPE for different cases including weak/strong interactions, defocusing/focusing nonlinearity, and zero/nonzero initial phase data are presented. In Section 5 a summary is given.

2. Gross–Pitaevskii equation

At temperatures T much smaller than the critical temperature T_c [35], a BEC is well described by the macroscopic wave function $\psi = \psi(\mathbf{x}, t)$ whose evolution is governed by a self-consistent, mean field nonlinear Schrödinger equation (NLSE) known as the Gross–Pitaevskii equation [31,44]. If a harmonic trap potential is considered, the equation becomes

$$\mathrm{i}\hbar\frac{\partial\psi(\mathbf{x},t)}{\partial t} = -\frac{\hbar^2}{2m}\nabla^2\psi(\mathbf{x},t) + \frac{m}{2}\left(\omega_x^2x^2 + \omega_y^2y^2 + \omega_z^2z^2\right)\psi(\mathbf{x},t) + NU_0|\psi(\mathbf{x},t)|^2\psi(\mathbf{x},t), \tag{2.1}$$

where $\mathbf{x} = (x, y, z)^{\mathrm{T}}$ is the spatial coordinate vector, m is the atomic mass, $\hbar$ is the Planck constant, N is the number of atoms in the condensate, and ω_x, ω_y and ω_z are the trap frequencies in x-, y- and z-direction, respectively. For the following we assume (w.r.o.g.) $\omega_x \leqslant \omega_y \leqslant \omega_z$. When $\omega_x = \omega_y = \omega_z$, the trap potential is isotropic. U_0 describes the interaction between atoms in the condensate and has the form

$$U_0 = \frac{4\pi\hbar^2 a}{m}, \tag{2.2}$$

where a is the s-wave scattering length (positive for repulsive interaction and negative for attractive interaction). It is necessary to ensure that the wave function is properly normalized. Specifically, we require

$$\int_{\mathbb{R}^3} |\psi(\mathbf{x},t)|^2\,\mathrm{d}\mathbf{x} = 1. \tag{2.3}$$

A typical set of parameters used in current experiments with ^{87}Rb is given by

$$m = 1.44\times10^{-25}\ (\mathrm{kg}),\quad \omega_x = \omega_y = \omega_z = 20\pi\ (\mathrm{rad/s}),\quad a = 5.1\times10^{-9}\ (\mathrm{m}),\quad N:\ 10^2 \sim 10^7 \tag{2.4}$$

and the Planck constant has the value

$$\hbar = 1.05\times10^{-34}\ (\mathrm{Js}).$$

2.1. Dimensionless GPE

In order to scale Eq. (2.1) under the normalization (2.3), we introduce

$$\tilde{t} = \omega_x t,\quad \tilde{\mathbf{x}} = \frac{\mathbf{x}}{x_s},\quad \tilde{\psi}(\tilde{\mathbf{x}},\tilde{t}) = x_s^{3/2}\psi(\mathbf{x},t), \tag{2.5}$$

where x_s is the characteristic 'length' of the condensate. Plugging (2.5) into (2.1), multiplying by $1/m\omega_x^2x_s^{1/2}$, and then removing all $\tilde{}$, we obtain the following dimensionless Gross–Pitaevskii equation under the normalization (2.3) in three spatial dimensions

$$\mathrm{i}\varepsilon\frac{\partial\psi(\mathbf{x},t)}{\partial t} = -\frac{\varepsilon^2}{2}\nabla^2\psi(\mathbf{x},t) + V(\mathbf{x})\psi(\mathbf{x},t) + \delta\varepsilon^{5/2}|\psi(\mathbf{x},t)|^2\psi(\mathbf{x},t), \tag{2.6}$$

where

$$V(\mathbf{x}) = \frac{1}{2}\left(x^2 + \gamma_y^2y^2 + \gamma_z^2z^2\right),$$

$$\varepsilon = \frac{\hbar}{\omega_x m x_s^2} = \left(\frac{a_0}{x_s}\right)^2, \quad \gamma_y = \frac{\omega_y}{\omega_x}, \quad \gamma_z = \frac{\omega_z}{\omega_x},$$

$$\delta = \frac{U_0 N}{a_0^3 \hbar \omega_x} = \frac{4\pi a N}{a_0}, \quad a_0 = \sqrt{\frac{\hbar}{\omega_x m}},$$

with a_0 the length of the harmonic oscillator ground state (in x-direction). The coefficient of the nonlinearity of (2.6) (interaction strength parameter) can also be expressed as

$$\kappa := \delta\varepsilon^{5/2} = \frac{4\pi a N}{a_0}\left(\frac{a_0}{x_s}\right)^5 = \frac{1}{2}\frac{8\pi a N}{x_s^3}\frac{a_0^4}{x_s^2} = \frac{\operatorname{sgn}(a)}{2}\frac{a_0^2}{x_{\mathrm{h}}^2}\frac{a_0^2}{x_s^2} = \frac{\operatorname{sgn}(a)}{2}\left(\frac{a_0}{x_{\mathrm{h}}}\frac{a_0}{x_s}\right)^2, \tag{2.7}$$

where x_{h} is the healing length [10] with

$$x_{\mathrm{h}} := \left(\frac{8\pi|a|N}{x_s^3}\right)^{-1/2}. \tag{2.8}$$

If we plug the typical set of parameter values (2.4) into the above parameters, we find

$$a_0 \approx 0.3407 \times 10^{-5}\ (\mathrm{m}), \quad \delta \approx 0.01881, \quad N: \ 1.881 \sim 188,100.$$

Remark 2.1. If one chooses $x_s = a_0$ in (2.5), then $\varepsilon = 1$ in (2.6), $\kappa = \delta$ in (2.7), and Eq. (2.6) takes the form often appearing in the physical literature. This choice for x_s is appropriate in the weak interaction regime characterized by $4\pi|a|N \ll a_0$ and in the moderate interaction regime where $4\pi|a|N \approx a_0$. In the strong interaction regime $4\pi|a|N \gg a_0$ a different choice is more appropriate, namely $x_s = (4\pi|a|Na_0^4)^{1/5}$, which gives $|\kappa| = 1$ and $\varepsilon = (a_0/4\pi|a|N)^{1/5} \ll 1$. Other choices for x_s, based on approximating the actual condensate length scale, shall be discussed in Section 2.2. Note that the choice of x_s determines the observation scale of the condensate and decides: (i) which phenomena are 'visible' by asymptotic analysis, (ii) which phenomena can be resolved by discretization on specified spatial/temporal grids.

Thus, there are two extreme regimes: one is when $\varepsilon = \mathrm{O}(1)$ ($\Longleftrightarrow a_0 = \mathrm{O}(x_s)$) and $\kappa = \delta\varepsilon^{5/2} = \mathrm{o}(1)$ ($\Longleftrightarrow 4\pi|a|N \ll a_0$), then Eq. (2.6) describes a weakly interacting condensate. The other is when $\varepsilon = \mathrm{o}(1)$ ($\Longleftrightarrow x_s \gg a_0$) and $\kappa = \delta\varepsilon^{5/2} = \mathrm{O}(1)$ (implying $4\pi|a|N \gg a_0$) (or $\varepsilon = 1$ and $\kappa = \delta\varepsilon^{5/2} = \delta$ with $|\delta| \gg 1$ by the rescaling $\mathbf{x} \to \varepsilon^{1/2}\mathbf{x}$, $\psi \to \psi/\varepsilon^{3/4}$), then (2.6) corresponds to a strongly interacting condensate (Thomas–Fermi regime [10]) or, equivalently, to the semiclassical regime. We recall that Eq. (2.6) is *regularly perturbed* in the case of weak interactions and *singularly perturbed* in the semiclassical regime. Analytical techniques of asymptotic analysis are available in both cases providing structural information on the solutions of (2.6) and on numerical discretization schemes (spatial/temporal grid control, control of the computational domain, error estimates in linearized cases).

2.2. Approximate ground state solution in 3d

To find a stationary state of (2.6), we write

$$\psi(\mathbf{x}, t) = \exp(-\mathrm{i}\mu t/\varepsilon)\phi(\mathbf{x}), \tag{2.9}$$

where μ is the chemical potential of the condensate. Inserting into (2.6) gives the following equation for $\phi(\mathbf{x})$:

$$\mu\phi(\mathbf{x}) = -\frac{\varepsilon^2}{2}\nabla^2\phi(\mathbf{x}) + V(\mathbf{x})\phi(\mathbf{x}) + \kappa|\phi(\mathbf{x})|^2\phi(\mathbf{x}), \quad \mathbf{x} \in \mathbb{R}^3, \tag{2.10}$$

under the normalization condition

$$\int_{\mathbb{R}^3} |\phi(\mathbf{x})|^2 \,\mathrm{d}\mathbf{x} = 1. \tag{2.11}$$

This is a nonlinear eigenvalue problem. The Bose–Einstein condensate ground-state wave function $\phi_g(\mathbf{x})$ is found by solving this eigenvalue problem under the normalization condition (2.11) with the minimal chemical potential μ_g. Usually, the ground state problem is formulated variationally. Define the energy functional

$$E(\phi) := \frac{\varepsilon^2}{2}\int_{\mathbb{R}^3} |\nabla\phi|^2 \,\mathrm{d}\mathbf{x} + \int_{\mathbb{R}^3} V(x)|\phi|^2 \,\mathrm{d}\mathbf{x} + \frac{\kappa}{2}\int_{\mathbb{R}^3} |\phi|^4 \,\mathrm{d}\mathbf{x}. \tag{2.12}$$

It is easy to see that critical points of E are 'eigenfunctions' of the nonlinear Hamiltonian. To compute the ground state ϕ_g we solve

$$E(\phi_g) = \min_{\int_{\mathbb{R}^3}|\phi|^2\,\mathrm{d}\mathbf{x}=1} E(\phi), \quad \mu_g = E(\phi_g) + \frac{\kappa}{2}\int_{\mathbb{R}^3} |\phi_g|^4 \,\mathrm{d}\mathbf{x}. \tag{2.13}$$

In the case of a defocusing (stable) condensate the energy functional $E(\psi)$ is positive, coercive and weakly lower semicontinuous on the unit sphere in $L^2(\mathbb{R}^3)$, thus the existence of a minimum follows from standard theory. For understanding the uniqueness question note that $E(\alpha\phi_g) = E(\phi_g)$ for all $\alpha \in \mathbb{C}$ with $|\alpha| = 1$. Thus an additional constraint has to be introduced to show uniqueness, e.g., ϕ_g real valued and $\phi_g(\mathbf{x}) > 0$ for all $\mathbf{x} \in \mathbb{R}^3$ (see [37]). For focusing (unstable) 3-dimensional condensates the energy functional $E(\psi)$ is not bounded from below on the unit sphere of $L^2(\mathbb{R}^3)$. Thus, an absolute minimum of $E(\psi)$ does not exist on $\{\psi \in L^2(\mathbb{R}^3) | \|\psi\|_{L^2}^2 = 1\}$. The interpretation of critical points (local minimum, saddle points obtained by min–max-theory) as physically relevant ground states is by no means clear.

Using (simple) perturbation methods, we present here the approximate ground state solution of (2.6) in the two extreme regimes of weak repulsive or attractive interactions and strong repulsive interactions (see [10,18] for a discussion in physical literature).

These approximate ground state solutions are used in reducing the 3d GPE to a 2d GPE and a 1d GPE – see the next subsection for details – and as initial data for the numerical solution of the time-dependent GPE in Section 4 (see the subsequent discussion).

For a weakly interacting condensate, i.e., $\varepsilon = \mathrm{O}(1)$ and $\kappa = \mathrm{o}(1)$, we drop the nonlinear term (i.e., the last term on the right-hand side of (2.6)) and find the harmonic oscillator equation

$$\mu\phi(\mathbf{x}) = -\frac{\varepsilon^2}{2}\nabla^2\phi(\mathbf{x}) + \frac{1}{2}\left(x^2 + \gamma_y^2 y^2 + \gamma_z^2 z^2\right)\phi(\mathbf{x}). \tag{2.14}$$

The ground state solution of (2.14) is

$$\mu_g^w = \frac{1+\gamma_y+\gamma_z}{2}\varepsilon, \quad \phi_g^w(\mathbf{x}) = \frac{(\gamma_y\gamma_z)^{1/4}}{(\pi\varepsilon)^{3/4}}\exp(-(x^2+\gamma_y y^2+\gamma_z z^2)/2\varepsilon). \tag{2.15}$$

It can be viewed as an approximate ground state solution of (2.6) in the case of a weakly interacting condensate, with an $\mathrm{O}(\kappa)$-error in approximating the chemical potential and ground state. From (2.15), we can see that the diameter of the ground state solution (computed according to the formula (4.2)) in the weakly interacting condensate is

$$x_{\mathrm{g}}^{w} = \mathrm{O}\left(\sqrt{\varepsilon}\right) = \mathrm{O}(1) \quad \text{(after the scaling (2.5))}.$$

Also we remark that the condensate widths in y- and z-directions of the approximate ground state ϕ_{g}^{w} are $\mathrm{O}(\sqrt{\varepsilon}/\sqrt{\gamma_y}) = \mathrm{O}(1/\sqrt{\gamma_y})$ and $\mathrm{O}(\sqrt{\varepsilon}/\sqrt{\gamma_z}) = \mathrm{O}(1/\sqrt{\gamma_z})$, respectively. Clearly, this is important for the control of the computational domain.

For a condensate with strong repulsive interactions, i.e., $\varepsilon = \mathrm{o}(1)$, $\kappa = \mathrm{O}(1)$ and $\kappa > 0$, we drop the diffusion term (i.e., the first term on the right-hand side of (2.6)) corresponding to the Thomas–Fermi approximation [10]:

$$\mu\phi(\mathbf{x}) = V(\mathbf{x})\phi(\mathbf{x}) + \kappa|\phi(\mathbf{x})|^2\phi(\mathbf{x}), \quad \mathbf{x} \in \mathbb{R}^3. \tag{2.16}$$

The ground state solution of (2.16) is the compactly supported function ϕ_{g}^{s}:

$$\mu_{\mathrm{g}}^{s} = \frac{\varepsilon}{2}\left(\frac{15\delta\gamma_y\gamma_z}{4\pi}\right)^{2/5} = \frac{1}{2}\left(\frac{15\kappa\gamma_y\gamma_z}{4\pi}\right)^{2/5}, \quad \phi_{\mathrm{g}}^{s}(\mathbf{x}) = \begin{cases} \sqrt{\left(\mu_{\mathrm{g}}^{s} - V(\mathbf{x})\right)/\kappa}, & V(\mathbf{x}) < \mu_{\mathrm{g}}^{s}, \\ 0, & \text{otherwise.} \end{cases} \tag{2.17}$$

This shows that the diameter of the ground state solution in the strongly interacting repulsive condensate is

$$x_{\mathrm{g}}^{s} = \sqrt{\mu_{\mathrm{g}}^{s}} = \mathrm{O}((\delta\gamma_y\gamma_z)^{1/5})\frac{a_0}{x_s} = \mathrm{O}\left(\left(\frac{4\pi|a|N\gamma_y\gamma_z}{a_0}\right)^{1/5}\right)\frac{a_0}{x_s} \quad \text{(again after the scaling (2.5))}.$$

Approximate widths of ϕ_{g}^{s} in the y and z-directions are $\mathrm{O}((\kappa\gamma_z)^{1/5}/\gamma_y^{4/5}) = \mathrm{O}(\gamma_z^{1/5}/\gamma_y^{4/5})$ and $\mathrm{O}((\kappa\gamma_y)^{1/5}/\gamma_z^{4/5}) = \mathrm{O}(\gamma_y^{1/5}/\gamma_z^{4/5})$, respectively.

This analysis suggests to choose the characteristic condensate length x_s such that the (dimensionless) ground state width x_{g}^{w} is $\mathrm{O}(1)$ after the scaling (2.5), i.e., $x_s = \mathrm{O}(a_0)$ for weak interaction (as in Remark 2.1) and $x_s = \mathrm{O}(((4\pi|a|N/a_0)\gamma_y\gamma_z)^{1/5}a_0)$ for strong repulsive interaction (different from Remark 2.1 if $\gamma_y \gg 1$ or $\gamma_z \gg 1$). If we use the typical set of parameter values (2.4) in the above identity, we obtain

$$\varepsilon: \ 0.0078 \sim 1.$$

Remark 2.2. The approximate ground state ϕ_{g}^{w} in the weak-interaction regime has finite energy, more precisely

$$E(\phi_{\mathrm{g}}^{w}) = \mu_{\mathrm{g}}^{w} + \frac{\kappa}{4}\left(\frac{\gamma_y\gamma_z}{\pi^3\varepsilon^3}\right)^{1/2} = \mu_{\mathrm{g}}^{w} + \mathrm{O}(\kappa) \tag{2.18}$$

as $\kappa \to 0$ for $\varepsilon = \mathrm{O}(1)$, $\gamma_z = \mathrm{O}(1)$, $\gamma_y = \mathrm{O}(1)$.

Contrarily the energy of the Thomas–Fermi approximation is infinite

$$E(\phi_{\mathrm{g}}^{s}) = +\infty \tag{2.19}$$

due to the low regularity of ϕ_{g}^{s} at the free boundary $V(x) = \mu_{\mathrm{g}}^{s}$. More precisely, ϕ_{g}^{s} is locally $C^{1/2}$ at the interface but not $H^1_{\mathrm{loc}}(\mathbb{R}^3)$. This is a typical behavior for solutions of free boundary value problems, which indicates that ϕ_{g}^{s} does not approximate ϕ_{g} to the full $\mathrm{O}(\varepsilon^2)$ – order, as indicated by formal consistency. An interface layer correction has to be constructed in order to improve the approximation quality. For a convergence proof of $\phi_{\mathrm{g}}^{s} \to \phi_{\mathrm{g}}$ (without convergence rate) we refer to [37].

It is of course tempting to use approximate ground states as initial data for the GPE when simulating Bose–Einstein condensation. In the weak interaction case this produces $\mathrm{O}(\kappa)$ – errors in time dependent simulations on $\mathrm{O}(1)$ time intervals. In the strong interaction case an initial wave function ϕ_{g}^{s} produces time – dependent solutions with infinite energy (which usually generates breathing modes, cf. Example 3 III

in Section 4.2) and the error in the wave function introduced by this is typically significantly larger than $O(\varepsilon^2)$.

2.3. Reduction to lower dimensions

In two important cases, the 3d Gross–Pitaevskii Eq. (2.6) can approximately be reduced to a lower dimensional PDE. For a disk-shaped condensate with small height, i.e.,

$$\omega_x \approx \omega_y, \quad \omega_z \gg \omega_x, \quad \Longleftrightarrow \quad \gamma_y \approx 1, \quad \gamma_z \gg 1, \tag{2.20}$$

the 3d GPE (2.6) can be reduced to a 2d GPE with $\mathbf{x} = (x, y)^{\mathrm{T}}$ by assuming that the time evolution does not cause excitations along the z-axis since these have a large energy of approximately $\hbar\omega_z$ compared to excitations along the x- and y-axis with energies of about $\hbar\omega_x$. To understand this, consider the total condensate energy $E[\psi(t)]$:

$$E[\psi(t)] = \frac{\varepsilon^2}{2}\int_{\mathbb{R}^3} |\nabla\psi(t)|^2\,\mathrm{d}\mathbf{x} + \frac{1}{2}\int_{\mathbb{R}^3}\left(x^2 + \gamma_y^2 y^2\right)|\psi(t)|^2\,\mathrm{d}\mathbf{x} + \frac{\gamma_z^2}{2}\int_{\mathbb{R}^3} z^2|\psi(t)|^2\,\mathrm{d}\mathbf{x} + \frac{\kappa}{2}\int_{\mathbb{R}^3}|\psi(t)|^4\,\mathrm{d}\mathbf{x}. \tag{2.21}$$

Multiplying (2.6) by $\overline{\psi_t}$ and integrating by parts show the energy conservation

$$E[\psi(t)] = E[\psi_{\mathrm{I}}] \quad \forall t, \tag{2.22}$$

where $\psi_{\mathrm{I}} = \psi(t = 0)$ is the initial function which may depend on all parameters ε, γ_y, γ_z and κ. Now assume that ψ_{I} satisfies

$$\frac{E[\psi_{\mathrm{I}}]}{\gamma_z^2} \to 0, \quad \text{as} \quad \gamma_z \to \infty. \tag{2.23}$$

Take a sequence $\gamma_z \to \infty$ (and keep all other parameters fixed). Since $\int_{\mathbb{R}^3} |\psi(t)|^2\,\mathrm{d}\mathbf{x} = 1$ we conclude from weak compactness that there is a positive measure $n^0(t)$ such that

$$|\psi(t)|^2 \rightharpoonup n^0(t) \quad \text{weakly as} \quad \gamma_z \to \infty.$$

Energy conservation implies

$$\int_{\mathbb{R}^3} z^2|\psi(t)|^2\,\mathrm{d}\mathbf{x} \to 0, \quad \text{as} \quad \gamma_z \to \infty$$

and thus we conclude concentration of the condensate in the plane $z = 0$:

$$n^0(x, y, z, t) = n_2^0(x, y, t)\delta(z),$$

where $n_2^0(t)$ is a positive measure on $\mathbb{R}^2$.

Now let $\psi_3 = \psi_3(z)$ be a wave-function with

$$\int_{\mathbb{R}} |\psi_3(z)|^2\,\mathrm{d}z = 1,$$

depending on γ_z such that

$$|\psi_3(z)|^2 \rightharpoonup \delta(z), \quad \text{as} \quad \gamma_z \to \infty. \tag{2.24}$$

Denote by S the subspace

$$S = \{\psi = \psi_2(x,y)\psi_3(z) | \psi_2 \in L^2(\mathbb{R}^2)\}$$

and let

$$\Pi : L^2(\mathbb{R}^3) \to S \subseteq L^2(\mathbb{R}^3)$$

be the projection on S:

$$(\Pi\psi)(x,y,z) = \psi_3(z) \int_{\mathbb{R}} \overline{\psi_3}(\sigma)\psi(x,y,\sigma)\,\mathrm{d}\sigma.$$

Now write Eq. (2.6) in the form

$$\mathrm{i}\varepsilon\psi_t = \mathscr{A}\psi + \mathscr{F}(\psi),$$

where $\mathscr{A}\psi$ stands for the linear part and $\mathscr{F}(\psi)$ for the nonlinearity. Applying Π to the GP-equation gives

$$\begin{aligned}\mathrm{i}\varepsilon(\Pi\psi)_t &= \Pi\mathscr{A}\psi + \Pi\mathscr{F}(\psi)\\ &= \Pi\mathscr{A}(\Pi\psi) + \Pi\mathscr{F}(\Pi\psi) + \Pi((\Pi\mathscr{A} - \mathscr{A}\Pi)\psi + (\Pi\mathscr{F}(\psi) - \mathscr{F}(\Pi\psi))).\end{aligned} \tag{2.25}$$

The projection approximation of (2.6) is now obtained by dropping the commutator terms. it reads

$$\mathrm{i}\varepsilon(\Pi\sigma)_t = \Pi\mathscr{A}(\Pi\sigma) + \Pi\mathscr{F}(\Pi\sigma), \tag{2.26}$$

$$(\Pi\sigma)(t=0) = \Pi\psi_{\mathrm{I}}, \tag{2.27}$$

or explicitly, with

$$(\Pi\sigma)(x,y,z,t) =: \psi_2(x,y,t)\psi_3(z), \tag{2.28}$$

we find

$$\mathrm{i}\varepsilon\frac{\partial\psi_2}{\partial t} = -\frac{\varepsilon^2}{2}\nabla^2\psi_2 + \frac{1}{2}\left(x^2 + \gamma_y^2 y^2 + C\right)\psi_2 + \left(\delta\varepsilon^{5/2}\int_{-\infty}^{\infty}\psi_3^4(z)\,\mathrm{d}z\right)|\psi_2|^2\psi_2, \tag{2.29}$$

where

$$C = \gamma_z^2\int_{-\infty}^{\infty} z^2|\psi_3(z)|^2\,\mathrm{d}z + \varepsilon^2\int_{-\infty}^{\infty}\left|\frac{\mathrm{d}\psi_3}{\mathrm{d}z}\right|^2\mathrm{d}z.$$

Since this GPE is time-transverse invariant, we can replace $\psi_2 \to \psi\exp(-\mathrm{i}(Ct/2\varepsilon))$ and drop the constant C in the trap potential. The observables are not affected by this.

The 'effective' GP-equation (2.29) is well known in the physical literature [36], where the projection method is often referred to as 'integrating out the z-coordinate'. However, an analysis of the limit process $\gamma_z \to \infty$ has to be based on the derivation as presented above, in particular on studying the commutators $\Pi\mathscr{A} - \mathscr{A}\Pi$, $\Pi\mathscr{F} - \mathscr{F}\Pi$. In the case of small interaction $\varepsilon = \mathrm{O}(1)$, $\kappa = \mathrm{o}(1)$, a good choice for $\psi_3(z)$ is the ground state of the harmonic oscillator in z-dimension:

$$\psi_3(z) = \left(\frac{\gamma_z}{\pi\varepsilon}\right)^{1/4}\exp(-\gamma_z z^2/(2\varepsilon)). \tag{2.30}$$

Note that $|\psi_3(z)|^2 \rightharpoonup \delta(z)$ as $\gamma_z \to \infty$ and that $\Pi\mathscr{A} = \mathscr{A}\Pi$ such that the error in approximating $\Pi\psi(t)$ by $\Pi\sigma$ is determined by the commutator of the nonlinearity, which is $\mathrm{O}(\kappa)$.

For condensates with other than small interaction the choice of ψ_3 is much less obvious. Often one assumes that the condensate density along the z-axis well described by the (x,y)-trace of the ground state position density $|\phi_g|^2$

$$|\psi(x,y,z,t)|^2 \approx |\psi_2(x,y,t)|^2 \int_{\mathbb{R}^2} |\phi_g(x_1,y_1,z)|^2 \,\mathrm{d}x_1\,\mathrm{d}y_1 \tag{2.31}$$

and (taking a pure-state-approximation)

$$\psi_3(z) = \left(\int_{\mathbb{R}^2} |\phi_g(x,y,z)|^2 \,\mathrm{d}x\,\mathrm{d}y \right)^{1/2}. \tag{2.32}$$

A mathematical analysis of the limit process $\gamma_z \to \infty$ is currently under study.

For a cigar-shaped condensate

$$\omega_y \gg \omega_x, \quad \omega_z \gg \omega_x, \quad \Longleftrightarrow \quad \gamma_y \gg 1, \quad \gamma_z \gg 1, \tag{2.33}$$

the 3d GPE (2.6) can be reduced to a 1d GPE by proceeding analogously.

Then the 3d GPE (2.6), 2d GPE and 1d GPE can then be written in a unified way

$$\mathrm{i}\varepsilon \frac{\partial \psi(\mathbf{x},t)}{\partial t} = -\frac{\varepsilon^2}{2}\nabla^2\psi(\mathbf{x},t) + V_d(\mathbf{x})\psi(\mathbf{x},t) + \kappa_d|\psi(\mathbf{x},t)|^2\psi(\mathbf{x},t), \quad \mathbf{x} \in \mathbb{R}^d, \tag{2.34}$$

where

$$\kappa_d = \delta\varepsilon^{5/2} \begin{cases} \int_{\mathbb{R}^2} \psi_{23}^4(y,z)\,\mathrm{d}y\,\mathrm{d}z, \\ \int_{\mathbb{R}} \psi_3^4(z)\,\mathrm{d}z, \\ 1, \end{cases}, \quad V_d(\mathbf{x}) = \begin{cases} \frac{1}{2}x^2, & d=1, \\ \frac{1}{2}\left(x^2+\gamma_y^2y^2\right), & d=2, \\ \frac{1}{2}\left(x^2+\gamma_y^2y^2+\gamma_z^2z^2\right), & d=3. \end{cases} \tag{2.35}$$

The normalization condition for (2.34) is

$$\int_{\mathbb{R}^d} |\psi(\mathbf{x},t)|^2 \,\mathrm{d}\mathbf{x} = 1. \tag{2.36}$$

By using the approximate ground state of Section 2.2, we derive – after simple calculations – for a weakly interacting condensate

$$\kappa_d := \kappa_d^w = \begin{cases} \frac{\kappa(\gamma_y\gamma_z)^{1/2}}{2\pi\varepsilon} = \delta\varepsilon^{3/2}\frac{(\gamma_y\gamma_z)^{1/2}}{2\pi}, & d=1, \\ \kappa\sqrt{\frac{\gamma_z}{2\pi\varepsilon}} = \delta\varepsilon^{4/2}\sqrt{\frac{\gamma_z}{2\pi}}, & d=2, \\ \kappa = \delta\varepsilon^{5/2}, & d=3, \end{cases} \tag{2.37}$$

and for a condensate with strong repulsive interactions

$$\kappa_d := \kappa_d^s = \begin{cases} \frac{\pi}{9}\left(\frac{15}{4\pi}\right)^{8/5}(\kappa\gamma_y\gamma_z)^{3/5} = \frac{(\delta\gamma_y\gamma_z)^{3/5}\varepsilon^{3/2}\pi}{9}\left(\frac{15}{4\pi}\right)^{8/5}, & d=1, \\ \frac{5}{7}\left(\frac{4\pi}{15}\right)^{1/5}\frac{(\kappa\gamma_z)^{4/5}}{\gamma_y^{1/5}} = (\delta\gamma_z)^{4/5}\varepsilon^{4/2}\left(\frac{4\pi}{15\gamma_y}\right)^{1/5}\frac{5}{7}, & d=2, \\ \kappa = \delta\varepsilon^{5/2}, & d=3. \end{cases} \tag{2.38}$$

We call a d-dimensional ($d=1$ or 2) condensate 'very weakly interacting', if $\varepsilon = \mathrm{O}(1)$ and $|\kappa_d| = |\kappa_d^w| \ll 1$, which implies $|\delta|\sqrt{\gamma_z} \ll 1$ in 2d and $|\delta|\sqrt{\gamma_y\gamma_z} \ll 1$ after reduction to 1d.

Remark 2.3. By using very elongated trapping potentials it is now possible to produce weakly interacting condensates that are 'truly' in the 1d regime and the assumption that the condensate wave function factorizes is fulfilled with high accuracy. In cases where the interactions cannot be neglected low dimensional simulations [48] should be viewed as model calculations where the effective interaction strength in the reduced equation is estimated by Eq. (2.37) for a weakly interacting condensate or (2.38) for a condensate with strong repulsive interactions. More detailed studies go beyond the GPE to describe low dimensional BEC's [36].

2.4. Geometrical optics $\varepsilon \to 0$

We set

$$\psi(\mathbf{x},t) = \sqrt{n(\mathbf{x},t)}\exp\left(\frac{\mathrm{i}}{\varepsilon}S(\mathbf{x},t)\right),$$

where $n = |\psi|^2$ and S is the phase of the wave-function. Inserting into the GP-equation (2.6) and separating real and imaginary parts give

$$n_t + \operatorname{div}(n\nabla S) = 0, \tag{2.39}$$

$$S_t + \frac{1}{2}|\nabla S|^2 + \kappa n + \frac{1}{2}\left(x^2 + \gamma_y^2 y^2 + \gamma_z^2 z^2\right) = \frac{\varepsilon^2}{2}\frac{1}{\sqrt{n}}\,\Delta\sqrt{n}. \tag{2.40}$$

Eq. (2.39) is the transport equation for the atom density and (2.40) the Hamilton–Jacobi equation for the phase.

By formally passing to the limit $\varepsilon \to 0$ (cf. [27]), we obtain the system

$$n_t^0 + \operatorname{div}(n^0\nabla S^0) = 0, \tag{2.41}$$

$$S_t^0 + \frac{1}{2}|\nabla S^0|^2 + \kappa n^0 + \frac{1}{2}\left(x^2 + \gamma_y^2 y^2 + \gamma_z^2 z^2\right) = 0. \tag{2.42}$$

It is well known that this limit process is only correct in the defocusing case $\kappa > 0$ before caustic onset, i.e., in time-intervals where the solution of the Hamilton–Jacobin equation (2.40) coupled with the atom-number conservation Eq. (2.39) is smooth. After the breakdown of regularity oscillations occur which make the term $(\varepsilon^2/2)(1/\sqrt{n})\Delta\sqrt{n}$ at least $O(1)$ such that the validity of the formal limit process is destroyed. The limiting behavior after caustics appear is not understood yet except in the one-dimensional case without confinement, see [34]. Also, the focusing case $\kappa < 0$ is not fully understood yet.

3. Numerical approximation

In this section we present a time-splitting Fourier spectral method, which was used by Bao et al. [6,7] to numerically solve the Schrödinger equation in the semiclassical regime. We reiterate that neither time splitting discretisations nor Fourier spectral methods are new, both have been applied successfully to many PDE problems [12,29,50]. Here we adapt the combination of both techniques to the GP equation and infer computational domain and mesh size controls from analytical (perturbation) results. The merit of this method is that it is unconditionally stable, time reversible, time-transverse invariant, and conserves the total particle number. Also, it has very favorable properties with respect to efficiently choosing the spatial/

temporal grid in dependence of the semiclassical parameter ε. For simplicity of notation we shall introduce the method in one space dimension ($d = 1$). Generalizations to $d > 1$ are straightforward for tensor product grids and the results remain valid without modifications. For $d = 1$, Eq. (2.34) with periodic boundary conditions becomes

$$\mathrm{i}\varepsilon\frac{\partial\psi(x,t)}{\partial t} = -\frac{\varepsilon^2}{2}\psi_{xx}(x,t) + \frac{x^2}{2}\psi(x,t) + \kappa_1|\psi(x,t)|^2\psi(x,t), \quad a < x < b, \tag{3.1}$$

$$\psi(x,t=0) = \psi^0(x), \quad a \leqslant x \leqslant b, \tag{3.2}$$

$$\psi(a,t) = \psi(b,t), \quad \psi_x(a,t) = \psi_x(b,t), \quad t > 0. \tag{3.3}$$

We choose the spatial mesh size $h = \Delta x > 0$ with $h = (b-a)/M$ for M an even positive integer, the time step $k = \Delta t > 0$ and let the grid points and the time step be

$$x_j := a + jh, \quad t_n := nk, \quad j = 0, 1, \ldots, M, \quad n = 0, 1, 2, \ldots$$

Let ψ_j^n be the approximation of $\psi(x_j, t_n)$ and ψ^n be the solution vector with components ψ_j^n.

3.1. Time-splitting spectral method (TSSP)

From time $t = t_n$ to $t = t_{n+1}$, the GPE (3.1) is solved in two splitting steps. One solves first

$$\mathrm{i}\varepsilon\psi_t = -\frac{\varepsilon^2}{2}\psi_{xx}, \tag{3.4}$$

for the time step of length k, followed by solving:

$$\mathrm{i}\varepsilon\frac{\partial\psi(x,t)}{\partial t} = \frac{x^2}{2}\psi(x,t) + \kappa_1|\psi(x,t)|^2\psi(x,t), \tag{3.5}$$

for the same time step, Eq. (3.4) will be discretized in space by the Fourier spectral method and integrated in time *exactly*. For $t \in [t_n, t_{n+1}]$, the ODE (3.5) leaves $|\psi|$ invariant in t [6,7] and therefore becomes

$$\mathrm{i}\varepsilon\frac{\partial\psi(x,t)}{\partial t} = \frac{x^2}{2}\psi(x,t) + \kappa_1|\psi(x,t_n)|^2\psi(x,t) \tag{3.6}$$

and thus can be integrated *exactly*. From time $t = t_n$ to $t = t_{n+1}$, we combine the splitting steps via the standard Strang splitting:

$$\begin{aligned}
&\psi_j^* = \exp(-\mathrm{i}(x_j^2/2 + \kappa_1|\psi_j^n|^2)k/(2\varepsilon))\psi_j^n,\\
&\psi_j^{**} = \frac{1}{M}\sum_{l=-M/2}^{M/2-1}\exp(-\mathrm{i}\varepsilon k\mu_l^2/2)\widehat{\psi}_l^*\exp(\mathrm{i}\mu_l(x_j-a)), \quad j = 0, 1, 2, \ldots, M-1,\\
&\psi_j^{n+1} = \exp(-\mathrm{i}(x_j^2/2 + \kappa_1|\psi_j^{**}|^2)k/(2\varepsilon))\psi_j^{**}, \quad j = 0, 1, 2, \ldots, M-1,
\end{aligned} \tag{3.7}$$

where $\widehat{\psi}_l^*$, the Fourier coefficients of ψ^*, are defined as

$$\mu_l = \frac{2\pi l}{b-a}, \quad \widehat{\psi}_l^* = \sum_{j=0}^{M-1}\psi_j^*\exp(-\mathrm{i}\mu_l(x_j-a)), \quad l = -\frac{M}{2}, \ldots, \frac{M}{2}-1. \tag{3.8}$$

The overall time discretization error comes solely from the splitting, which is second order in k for fixed $\varepsilon > 0$. The spatial discretization is of spectral (i.e., 'infinite') order of accuracy for $\varepsilon > 0$ fixed. An error analysis for linear Schrödinger equations taking into account the ε-dependence of the global error can be found in [6] (where it is shown that $k = \mathrm{O}(1)$ and $h = ((b-a)/M) = \mathrm{O}(\varepsilon)$ give correct observable), numerical tests for nonlinear problems in the semiclassical regimes in [7]. More restrictive meshing strategies are typically necessary in nonlinear cases, cf. Section 4.1.

For comparison purposes we review now alternative numerical methods [2,15,24] which are currently used for solving the Gross–Pitaevskii equation of BEC. One is the Crank–Nicolson finite difference (CNFD) scheme [2]:

$$\frac{\psi_j^{n+1}-\psi_j^n}{k} = \frac{\mathrm{i}\varepsilon}{4h^2}\left[\psi_{j+1}^{n+1} - 2\psi_j^{n+1} + \psi_{j-1}^{n+1} + \psi_{j+1}^n - 2\psi_j^n + \psi_{j-1}^n\right] - \frac{\mathrm{i}x_j^2}{4\varepsilon}(\psi_j^{n+1}+\psi_j^n) - \frac{\mathrm{i}\kappa_1}{2\varepsilon}|\psi_j^n|^2(\psi_j^{n+1}+\psi_j^n),$$
$$j = 1, 2, \ldots, M,$$

$$\psi_0^{n+1} = \psi_M^{n+1}, \quad \psi_{M+1}^{n+1} = \psi_1^{n+1},$$

$$\psi_j^0 = \psi_0(x_j), \quad j = 0, 1, \ldots, M.$$

Another one is the Crank–Nicolson spectral (CNSP) method:

$$\frac{\psi_j^{n+1}-\psi_j^n}{k} = \frac{\mathrm{i}\varepsilon}{4}\left[D_{xx}^f\psi^{n+1}\big|_{x=x_j} + D_{xx}^f\psi^n\big|_{x=x_j}\right] - \frac{\mathrm{i}x_j^2}{4\varepsilon}(\psi_j^{n+1}-\psi_j^n) - \frac{\mathrm{i}\kappa_1}{2\varepsilon}|\psi_j^n|^2(\psi_j^{n+1}+\psi_j^n),$$

$$\psi_j^0 = \psi_0(x_j), \quad j = 0, 1, \ldots, M,$$

where D_{xx}^f, a spectral differential operator approximation of ∂_{xx}, is defined as

$$D_{xx}^f U\big|_{x=x_j} = -\sum_{l=-M/2}^{M/2-1} \mu_l^2 (\widehat{U})_l \exp(\mathrm{i}\mu_l(x_j - a)). \tag{3.9}$$

Both methods are unconditionally stable, time reversible, conserve the total particle number but they are *not* time transverse-invariant. We do not present comparism tests with fully implicit and fully explicit finite difference methods since they are not at all competitive with the time splitting-spectral method. Generally: (1) they require severe stability constraints on the mesh sizes, (2) they do not conserve the total particle number, (3) they are not time transverse invariant. For a mathematical analysis of FD-methods for Schrödinger type equations in semiclassical regimes we refer to [39,40].

4. Numerical examples

In this section, we first perform a numerical comparison of TSSP, CNFD and CNSP in terms of accuracy and mesh size strategy for a 1d defocusing GPE. Then we apply the TSSP for solving 1d, 2d and 3d GPEs of Bose–Einstein condensation. Furthermore we also give a physical discussion on our numerical results.

In our computations, the initial condition for (2.34) is always chosen in WKB form:

$$\psi(\mathbf{x}, t=0) = \psi^0(\mathbf{x}) = A^0(\mathbf{x})\exp(\mathrm{i}S^0(\mathbf{x})/\varepsilon) \tag{4.1}$$

with A^0 and S^0 real valued, regular and with $A^0(\mathbf{x})$ decaying to zero sufficiently fast as $|\mathbf{x}| \to \infty$. We compute with TSSP on a domain, which is large enough (as controlled by the initial data) such that the periodic boundary conditions do not introduce a significant aliasing error relative to the whole space problem. There are certainly more sophisticated analysis for controlling aliasing errors, however these do not significantly improve the results for exponentially decaying initial densities.

To quantify the numerical results, we define the condensate widths along the x-, y- and z-axis as

$$\sigma_x = \sqrt{\langle (x - \langle x \rangle)^2 \rangle}, \quad \sigma_y = \sqrt{\langle (y - \langle y \rangle)^2 \rangle}, \quad \sigma_z = \sqrt{\langle (z - \langle z \rangle)^2 \rangle}, \tag{4.2}$$

where brackets denote space averaging with respect to the position density

$$\langle f \rangle \equiv \int_{\mathbb{R}^d} f(\mathbf{x}) |\psi(\mathbf{x}, t)|^2 \, d\mathbf{x}.$$

4.1. Comparisons of different methods

Example 1. 1d Defocusing condensate, i.e., we choose $d = 1$ in (2.34) with positive κ_1. The initial condition is taken as

$$\psi(x, 0) = \frac{1}{(\pi\varepsilon)^{1/4}} \exp(-x^2/(2\varepsilon)), \quad x \in \mathbb{R}. \tag{4.3}$$

We choose $\varepsilon = 0.1$ and $\kappa_1 = 1.2649$ and solve this problem on $[-16, 16]$, i.e., $a = -16$ and $b = 16$ with periodic boundary conditions. Let ψ be the 'exact' solution which is obtained numerically by using TSSP with a very fine mesh and time step, e.g., $h = \frac{1}{256}$ and $k = 0.00001$, and $\psi_{h,k}$ be the numerical solution obtained by using a method with mesh size h and time step k.

First we compare the discretization error in space. We choose a very small time step, e.g., $k = 0.00002$ such that the error from the time discretization is negligible compared to the spatial discretization error, and solve the GPE using different methods and varying spatial mesh sizes h. Table 1 lists the numerical errors $\|\psi(t) - \psi_{h,k}(t)\|_{l^2}$ at $t = 2$ for varying spatial mesh sizes h. Clearly TSSP and CNSP show roughly the same errors due to the fact that the temporal discretization is almost 'exact'.

Secondly, we test the discretization error in time. Again, we take $\varepsilon = 0.1$ and $\kappa_1 = 1.2649$. Table 2 shows the numerical errors $\|\psi(t) - \psi_{h,k}(t)\|_{l^2}$ at $t = 2$ with a very small mesh size $h = \frac{1}{32}$ for different time steps k and different numerical methods. Here, CNSP and CNFD show almost no difference since the spatial discretization now is almost 'exact'.

We also tested numerically the unconditional stability of the time-splitting spectral method, which was already proven rigorously in [6]. Numerical tests showed no significant accumulation of round-off errors

Table 1
Spatial discretization error analysis: $\|\psi(t) - \psi_{h,k}(t)\|_{l^2}$ at time $t = 2$ under $k = 0.00002$

Mesh	$h = \frac{1}{4}$	$h = \frac{1}{8}$	$h = \frac{1}{16}$	$h = \frac{1}{32}$	CPU time (s)
TSSP	0.2248	2.048E − 2	3.641E − 5	7.982E − 10	0.01
CNSP	0.2248	2.048E − 2	3.642E − 5	8.538E − 8	15.54
CNFD	0.6314	0.3380	8.784E − 2	2.801E − 2	1.27

The CPU time is counted at the same accuracy (i.e., $\|\psi(2) - \psi_{h,k}(2)\|_{l^2} \approx 3.65\text{E} - 5$) and on an AlphaServer DS20 workstation. For that accuracy, TSSP needs $h = \frac{1}{16}$ and $k = 0.001$, CNSP needs $h = \frac{1}{16}$ and $k = 0.00002$ and CNFD needs $h = \frac{1}{1024}$ and $k = 0.00001$.

Table 2
Time discretization error analysis: $\|\psi(t) - \psi_{h,k}(t)\|_{l^2}$ at time $t = 2$ under $h = \frac{1}{32}$

Time step	$k = 0.05$	$k = 0.025$	$k = 0.0125$	$k = 0.00625$
TSSP	1.112E − 2	1.716E − 3	4.021E − 4	1.045E − 4
CNSP	0.5215	0.1247	4.363E − 2	1.565E − 2
CNFD	0.5344	0.13720	6.121E − 2	3.723E − 2

and conservation of the discrete l^2-norm was observed up to 10 significant digits for tests performed with $h = \frac{1}{32}$ and $k = 0.2$, $k = 0.05$, $k = 0.01$ computing up to $t = 4$.

At last, we test the ε-resolution of different methods. Here we shall compare the meshing strategies required in order to get the 'correct' condensate density $|\psi|^2$, for different methods when decreasing the semiclassical parameter ε. Fig. 1 shows the numerical results with different combinations of ε, h, k for different methods. Furthermore Fig. 2 shows the evolution of $\rho = |\psi|^2$ in space–time and the condensate width as a function of time by using TSSP for $\varepsilon = 0.1$ and $\kappa_1 = 1.2649$.

From Tables 1, 2 and Fig. 1, one can make the following observations:

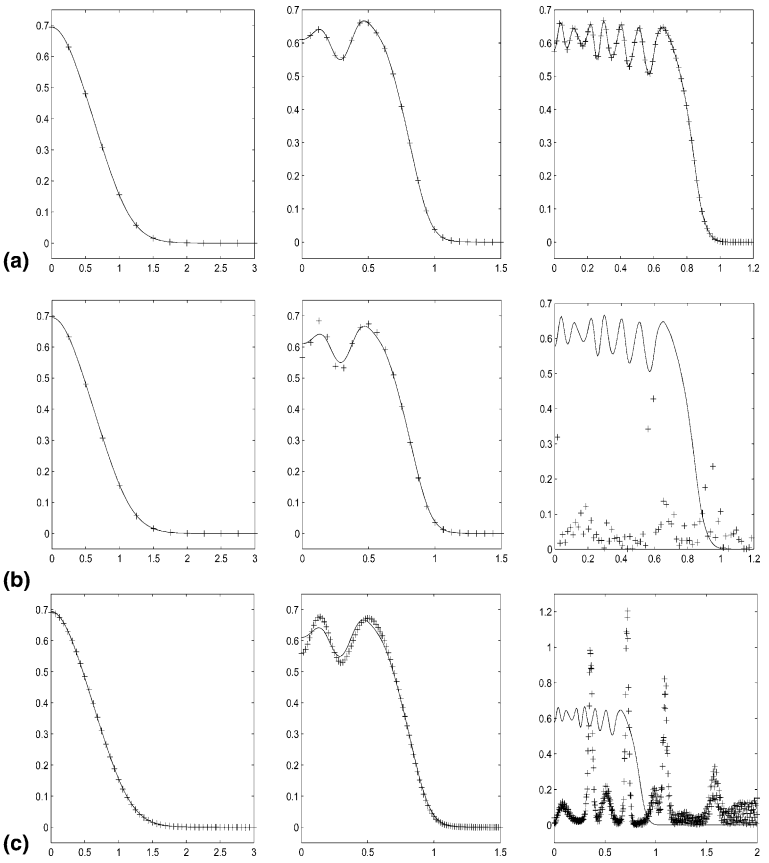

Fig. 1. ε-Resolution comparison in Example 1 for condensate density $|\psi|^2$ of different methods, '—': 'exact' solution, '+ + +': numerical solution. (a) TSSP: $\varepsilon = 0.4$, $h = \frac{1}{4}$, $k = 0.04$ (left); $\varepsilon = 0.1$, $h = \frac{1}{16}$, $k = 0.01$ (middle); and $\varepsilon = 0.025$, $h = \frac{1}{64}$, $k = 0.0025$ (right). (b) CNSP: $\varepsilon = 0.4$, $h = \frac{1}{4}$, $k = 0.02$ (left); $\varepsilon = 0.1$, $h = \frac{1}{16}$, $k = 0.005$ (middle); and $\varepsilon = 0.025$, $h = \frac{1}{64}$, $k = 0.00125$ (right). (c) CNFD: $\varepsilon = 0.4$, $h = \frac{1}{16}$, $k = 0.02$ (left); $\varepsilon = 0.1$, $h = \frac{1}{64}$, $k = 0.005$ (middle); and $\varepsilon = 0.025$, $h = \frac{1}{256}$, $k = 0.00125$ (right).

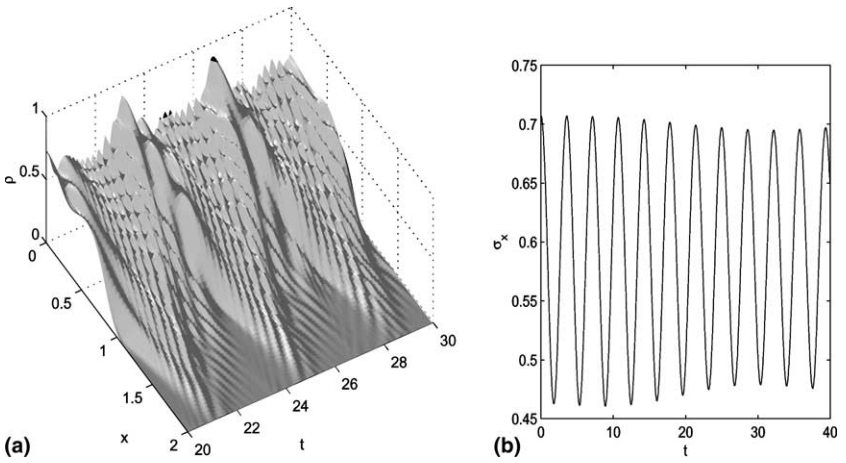

Fig. 2. Numerical results in Example 1 for $\varepsilon = 0.1$ and $\kappa_1 = 1.2649$. (a) Evolution of the position density; (b) widths of the condensate as a function of time.

(1) For TSSP, the spatial and temporal discretization errors are of spectral and second order accuracy, respectively. The admissible meshing strategy for obtaining the 'correct' condensate density in the defocusing case is: $h = O(\varepsilon)$ and $k = O(\varepsilon)$. This method is explicit, unconditional stable and its extension to 2d and 3d cases is straightforward without additional numerical difficulty.

(2) For CNSP, the spatial and temporal discretization errors are also of spectral and first order accuracy, respectively. But the admissible meshing strategy is: $h = O(\varepsilon)$ and $k = o(\varepsilon)$. Furthermore this method is implicit and its extension to the 2d or 3d case is expensive except when an ADI technique is used, which destroys the spatial spectral accuracy.

(3) For CNFD, the spatial and temporal discretization errors are of second and first order, respectively, and the admissible meshing strategy is: $h = o(\varepsilon)$ and $k = o(\varepsilon)$ (see [39]). This method is implicit and the remark of (2) applies.

Furthermore, the storage requirement of TSSP is less than the other two methods. The number of operations needed per time step is $O(M \ln M)$ for TSSP, at least $O(M^2)$ for CNSP, and $O(M)$ for CNFD when an ADI technique is used in 2d and 3d, where M is the total number of unknowns. To attain the same order of accuracy, CNFD needs many more grid points than TSSP.

4.2. Applications

Example 2. 2d Defocusing condensate, i.e., we choose $d = 2$ in (2.34). We solve this problem on $[-8, 8]^2$ with mesh size $h = \frac{1}{32}$ and time step $k = 0.001$. We present computations for four cases:

(I) O(1)-interactions, zero initial phase data

$$\varepsilon = 1.0, \quad \gamma_y = 1.0, \quad \kappa_2 = 2.0(\gamma_z = 10.0,\ \delta = 1.586), \quad \psi(x, y, 0) = \frac{1}{\sqrt{\pi\varepsilon}} \exp(-(x^2 + y^2)/(2\varepsilon)).$$

(II) Very weak interactions, anisotropic condensate, nonzero initial phase

$$\varepsilon = 1.0, \quad \gamma_y = 2.0, \quad \kappa_2 = 0.1(\gamma_z = 10.0,\ \delta = 0.0793),$$

$$\psi(x, y, 0) = \frac{\gamma_y^{1/4}}{\sqrt{\pi\varepsilon}} \exp(-(x^2 + \gamma_y y^2)/(2\varepsilon)) \exp(\mathrm{i}\cosh\left(\sqrt{x^2 + 2y^2}\right)/\varepsilon).$$

(III) Strong interactions, nonzero initial phase data

$$\varepsilon = 0.1, \quad \gamma_y = 1.0, \quad \mu_2^s = \sqrt{\kappa_2\gamma_y/\pi}, \quad \kappa_2 = 1.2649(\gamma_z = 10.0,\ \delta = 65.5227),$$

$$\psi(x,y,0) = \begin{cases} \sqrt{(\mu_2^s - (x^2+y^2)/2)/\kappa_2}\, e^{i\cosh\left(\sqrt{x^2+2y^2}\right)/\varepsilon}, & x^2+y^2 < 2\mu_2^s, \\ 0, & \text{otherwise.} \end{cases}$$

(IV) O(1)-interactions, anisotropic condensate with changing trap frequency

$$\varepsilon = 1.0, \quad \gamma_y = 2.0, \quad \varepsilon_1 = 2.0, \quad \kappa_2 = 2.0(\gamma_z = 10.0,\ \delta = 1.586),$$

$$\psi(x,y,0) = \frac{\gamma_y^{1/4}}{\sqrt{\pi\varepsilon_1}} \exp(-(x^2+\gamma_y y^2)/(2\varepsilon_1)).$$

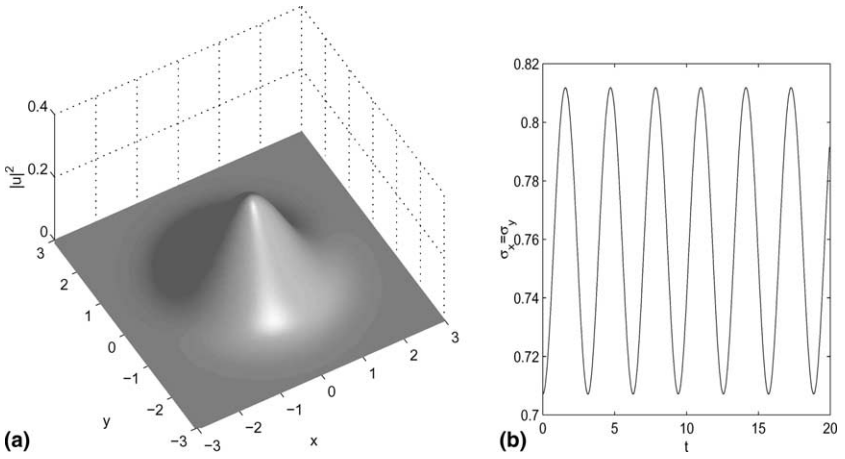

Fig. 3. Numerical results in Example 3 for case I. (a) Surface plot of the position density at $t = 40$; (b) widths of the condensate as a function of time.

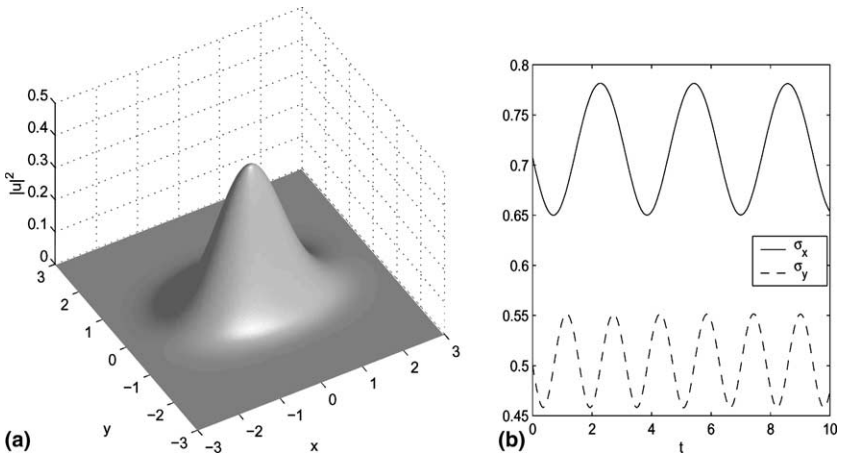

Fig. 4. Numerical results in Example 3 for case II. (a) Surface plot of the position density at $t = 40$; (b) widths of the condensate as a function of time.

Fig. 3 shows the surface plot of $\rho = |\psi|^2$ (labeled as $|u|^2$ in the figures) at time $t = 40$ and the condensate widths as a function of time for case I. Furthermore, Fig. 4 shows similar results for case II, Fig. 5 for case III, Figs. 6 and 7 for case IV.

Example 3. 2d Focusing condensate, i.e., we choose $d = 2$ in in (2.34). We solve this problem on $[-10, 10]^2$ with mesh size $h = \frac{1}{51.2}$ and time step $k = 0.00005$. We present computations for three cases:

(I) O(1)-interactions, positive initial energy

$$\varepsilon = 1.0, \quad \gamma_y = 1.0, \quad \kappa_2 = -2.0(\gamma_z = 10.0,\ \delta = -1.586), \quad \psi(x, y, 0) = \frac{1}{\sqrt{\pi\varepsilon}} \exp(-(x^2 + y^2)/(2\varepsilon)).$$

(II) Strong interactions, negative initial energy

$$\varepsilon = 0.3, \quad \gamma_y = 1.0, \quad \kappa_2 = -1.9718\ (\gamma_z = 10.0,\ \delta = -7.545),$$

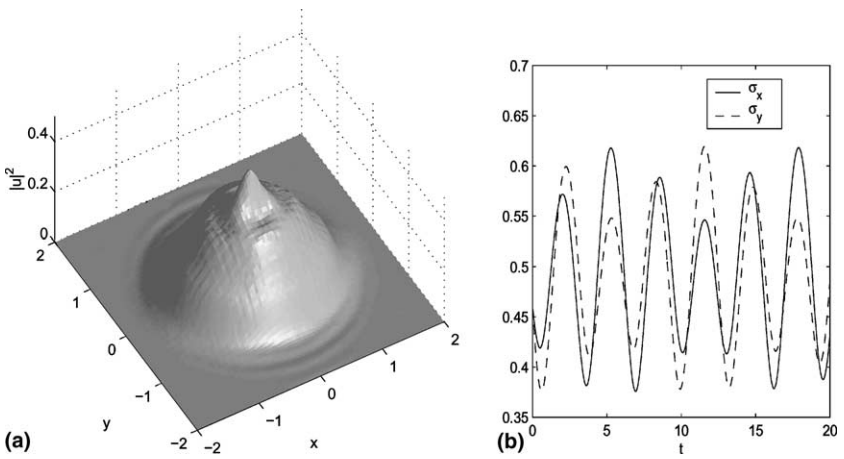

Fig. 5. Numerical results in Example 3 for case III. (a) Surface plot of the position density at $t = 40$; (b) widths of the condensate as a function of time.

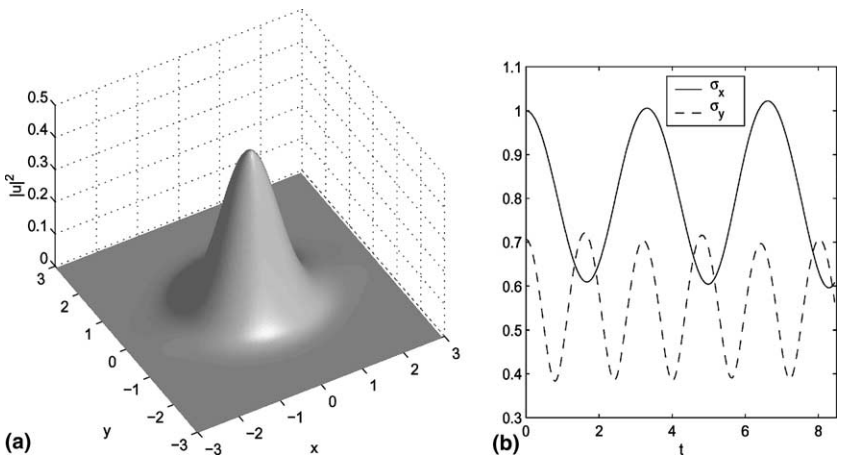

Fig. 6. Numerical results in Example 3 for case IV. (a) Surface plot of the position density at $t = 6.8$; (b) widths of the condensate as a function of time.

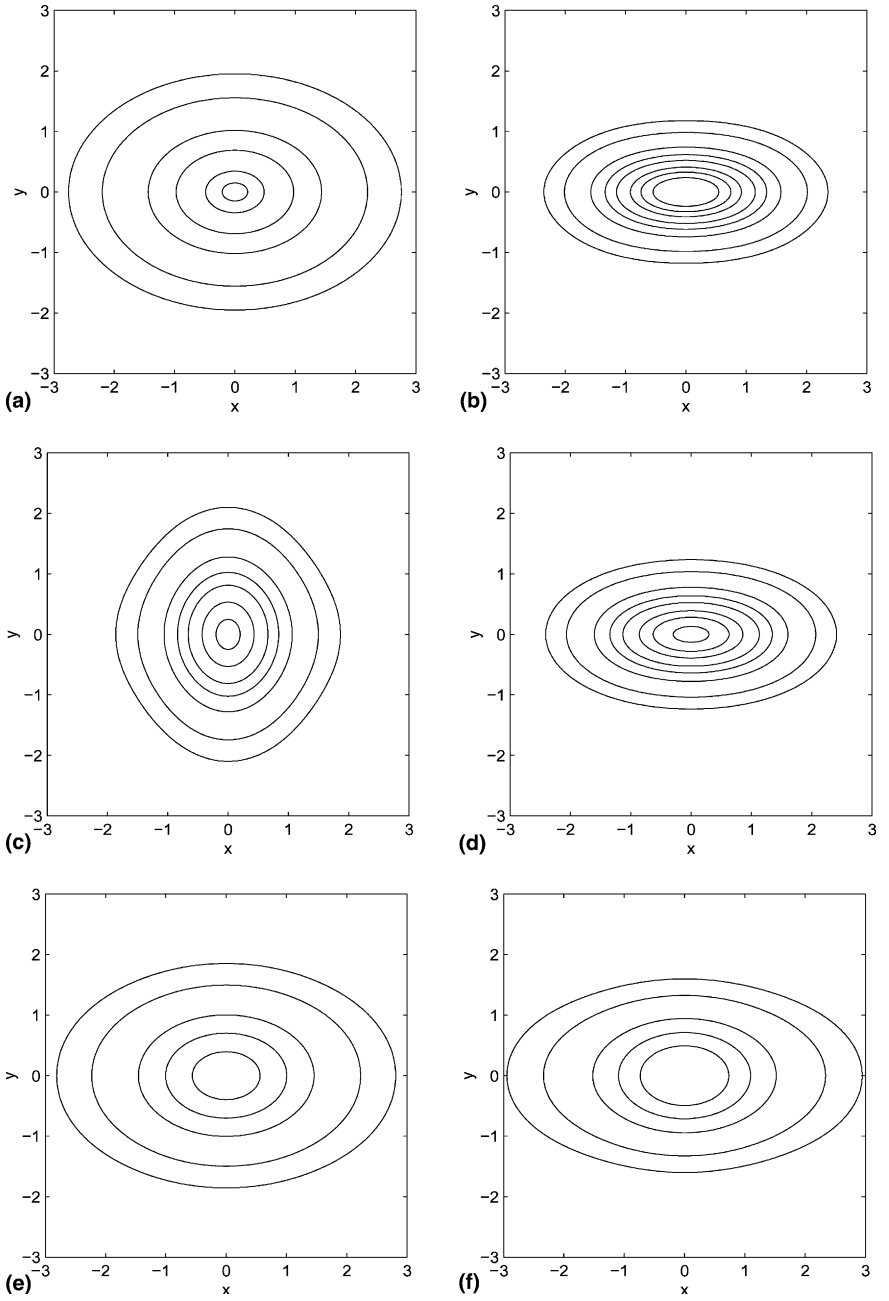

Fig. 7. Contour plots of the position density at different times in Example 3 for case IV. (a) $t = 0.0$, (b) $t = 0.85$, (c) $t = 1.7$, (d) $t = 2.55$, (e) $t = 3.4$, (f) $t = 6.8$.

$$\psi(x, y, 0) = \frac{1}{\sqrt{\pi\varepsilon}} \exp(-(x^2 + y^2)/(2\varepsilon)).$$

Fig. 8 shows the surface plot of $\rho = |\psi|^2$ at time $t = 40$ and the condensate widths as a function of time for case I. Furthermore, Fig. 9 for case II.

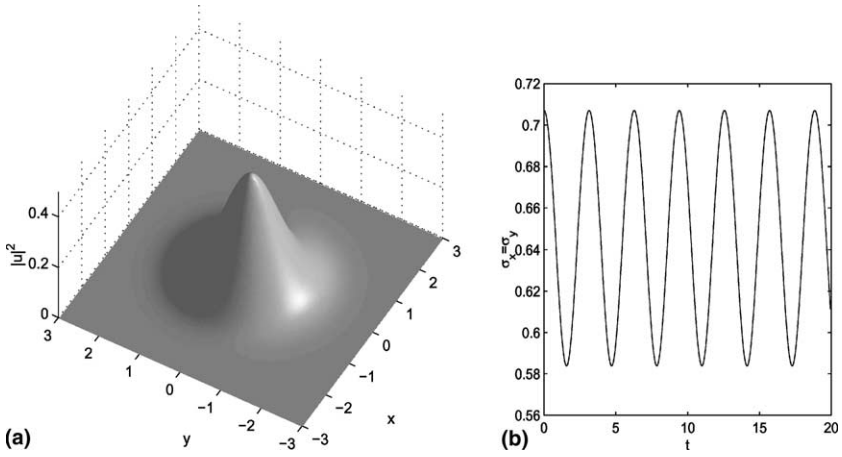

Fig. 8. Numerical results in Example 4 for case I. (a) Surface plot of the position density at $t = 40$; (b) widths of the condensate as a function of time.

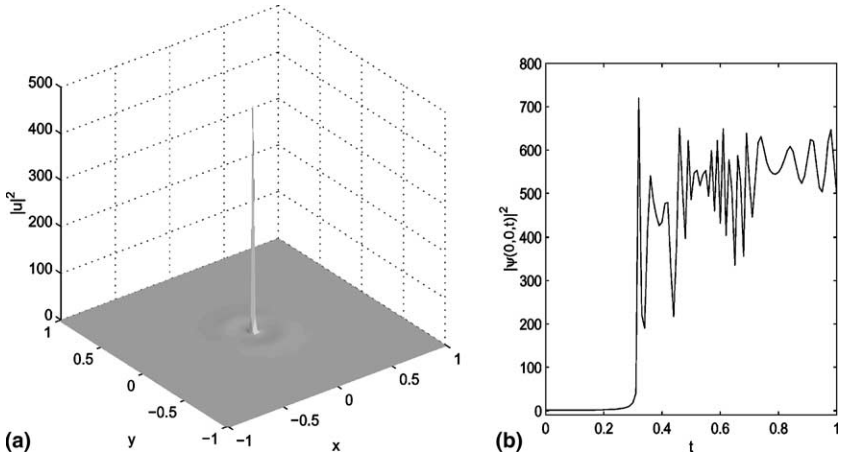

Fig. 9. Numerical results in Example 4 for case II. (a) Surface plot of the position density at $t = 0.5$; (b) peak of the position density $|\psi(0,0,t)|^2$ as a function of time.

Example 4. 3d Defocusing condensate, i.e., we choose $d = 3$ in in (2.34). We solve for $\mathbf{x} \in [-8,8]^3$ with mesh size $h = \frac{1}{8}$ and time step $k = 0.001$ and present computations for two cases:

(I) Anisotropic condensate with changing trap frequency

$$\varepsilon = 1.0, \quad \gamma_y = 2.0, \quad \gamma_z = 4.0, \quad \varepsilon_1 = \frac{1}{4}, \quad \kappa_3 = 0.1(\delta = 0.1),$$

$$\psi(x,y,z,0) = \frac{(\gamma_y\gamma_z)^{1/4}}{\sqrt{(\pi\varepsilon_1)^{3/4}}} \exp(-(x^2 + \gamma_y y^2 + \gamma_z z^2)/(2\varepsilon_1)).$$

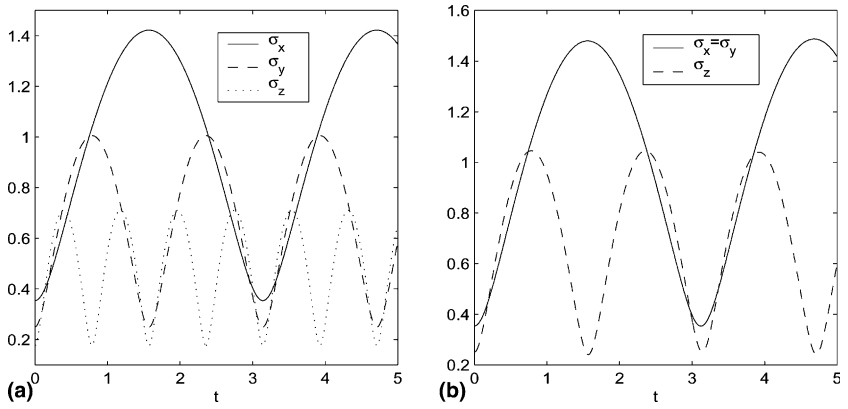

Fig. 10. Widths of the condensate as a function of time in Example 5. (a) For case I; (b) for case II.

(II) Cylindrically symmetric condensate with changing trap frequency

$$\varepsilon = 1.0, \quad \gamma_y = 1.0, \quad \gamma_z = 2.0, \quad \varepsilon_1 = \frac{1}{4}, \quad \kappa_3 = 1.0 \ (\delta = 1.0),$$

$$\psi(x,y,z,0) = \frac{(\gamma_y\gamma_z)^{1/4}}{\sqrt{(\pi\varepsilon_1)^{3/4}}} \exp(-(x^2 + \gamma_y y^2 + \gamma_z z^2)/(2\varepsilon_1)).$$

Fig. 10 shows the condensate widths as a function of time for cases I and II.

Example 5. 2d Vortices in BEC. We choose $d = 2$ and simulate the effect of stirring the (stable) condensate by adding a narrow, circularly moving Gaussian potential $W(\mathbf{x}, t)$ to the stationary trap potential in (2.34). $W(\mathbf{x}, t)$ represents, for example, a far-blue-detuned laser [13]. We set

$$W(\mathbf{x}, t) = W_s(t) \exp\Big[-4|\mathbf{x} - \mathbf{x}_s(t)|^2/V_s^2\Big],$$

with the center $\mathbf{x}_s(t) = (r_0 \cos \omega_s t, r_0 \sin \omega_s t)$ moving on a circle with radius r_0 and frequency ω_s. We start the simulation with the ground state in 2 dimensions (no stirrer at $t = 0$) and minimize transient effects by increasing the stirrer amplitude $W_s(t)$ linearly from 0 at $t = 0$ to a final value $W_s(t = \pi) =: W_f$ at $t = \pi$. The stirrer is then linearly withdrawn from $t = 4\pi$ to $t = 5\pi$ (after constant stirring, i.e., $W_s(t) = W_f$ for $\pi \leqslant t \leqslant 4\pi$) and the condensate is left to evolve freely after $t = 5\pi$. We recall that 2d and 3d vortices simulations were already performed in [3,13,14], here we present this example in order to put our numerical method to an important physical test.

We take the numerical values $\varepsilon = 1/\sqrt{50}$, $\kappa_d = 1$, $\gamma_y = 1$, $W_f = \sqrt{2}$, $V_s = 1/50^{1/4}$, $r_0 = 2/50^{1/4}$ and $\omega_s = 1$ for our simulation. We remark that a vortex in the condensate is a point $\mathbf{x}_w$ with $\psi(\mathbf{x}_w) = 0$ *and* singular or undefined phase.

In Fig. 11, we show the contour plot of the density $|\psi(\mathbf{x}, t)|^2$ at $t = 12\pi$ (where the fluid has already settled down after the stirring) and x, y-sectional plots of the vortex centered at $(x \approx -0.141, y \approx -0.229)$. In fact three vortices (labeled by 'X'), located at $(-0.141, -0.229)$, $(1.093, -0.0353)$ and $(0.282, 1.481)$ were identified. For an analysis of vortex-formation in semiclassical limits of the Schrödinger equation we refer to [38].

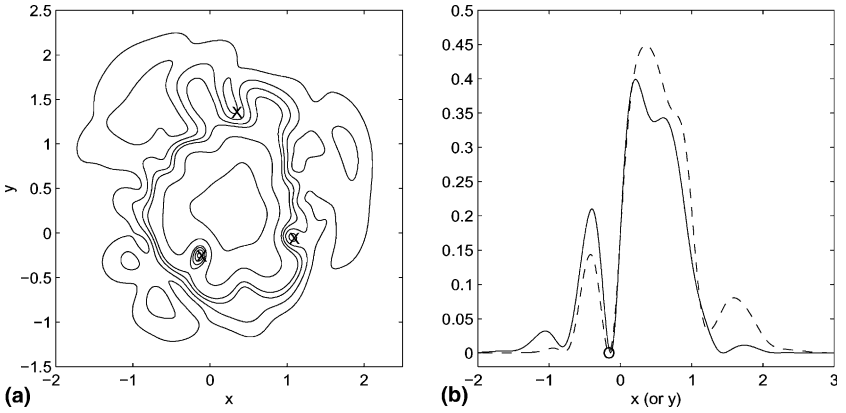

Fig. 11. Numerical results at time $t = 12\pi$ in Example 6. (a) Contour plot of the density function $|\psi|^2$ (three vortices were identified and labelled by 'X'); (b) x, y-sectional plot at a vortex (center of it is labelled by 'O') located at $(-0.141, -0.229)$; '—': $|\psi(x, -0.229, 12\pi)|^2$, '- - -': $|\psi(-0.141, y + 0.088, 12\pi)|^2$.

4.3. Discussion

In Section 4.1 we compared different numerical methods for solving the GPE with the TSSP. Now we complete our investigation on the validity of using the TSSP for solving the GPE by comparing the results obtained in Section 4.2 with well known properties of Bose–Einstein condensates at very low temperatures.

In Example 1 we present 1d simulations. Initially the condensate is assumed to be in its noninteracting ground state when at $t = 0$ repulsive interaction is turned on. In current experiments a change in the interaction strength can be achieved by applying external magnetic fields. Close to a Feshbach resonance the interaction strength shows a strong dependence on the magnetic field and even its sign can be changed by an appropriate choice of the magnetic field [45]. At the same time we also change the trap potential by setting $\varepsilon = 0.1$. These sudden changes lead to many rapid oscillations in the condensates (cf. Fig. 2(a)). The dominant excitation caused by the interactions is, as expected [23,33], the oscillation of the condensate width at approximately twice the trap frequency (cf. Fig. 2(b)).

Example 2 presents 2d simulations for various cases. In cases I there are $O(1)$ – interactions and in case II we investigate a weakly interacting condensate. We assume the condensate to be initially in the noninteracting ground state with possibly a nonuniform phase. As in Example 1 turning on the interactions causes the condensate to oscillate at approximately twice the corresponding trap frequency. Higher excitations like in Fig. 2(a) are not visible in Figs. 3(a), 4(a) since compared to Example 1 the strength of the interactions is much smaller. A nonuniform phase like in II causes the amplitude of the oscillations to be different in x and y direction. Note also that while in case I the condensate immediately starts to expand (cf. Fig. 3(b)) (due to the repulsive interactions) it starts to contract for the initial condition with a nonzero phase in case II. In case III we investigate the evolution of a strongly interacting condensate initially in the (approximate) Thomas Fermi ground state with an additional phase. Again, since this is not the exact ground state (see Remark 2.2) the width of the condensate starts to oscillate at about twice the trap frequency (cf. Fig. 5(a). In this case, however, due to the strong nonlinearity the oscillations along the x and y direction are coupled with each other as can be seen from Fig. 5(b). In case IV we investigate the effect of changing the trap frequency and turning on repulsive interactions (see Fig. 6). Like in the previous cases we find the dominant effect to be oscillations at about twice the corresponding trap frequency. The condensate initially starts to contract since the trap frequencies are increased at $t = 0$. For the initial conditions chosen in this case the amplitudes are sufficiently large to swap the widths σ_x and σ_y (cf. Fig. 7), whereas for small

changes in the trap frequency no swapping of the condensate widths would occur. The numerical results for the oscillations of a BEC obtained in Example 2 agree very well with experimental and theoretical results [23,33].

In Example 3 we show solutions for a focusing nonlinearity in 2d. Case I shows the effect of turning on $O(1)$ attractive interactions which leads to oscillations similar to those discussed in the previous examples (see Fig. 8). In case II a condensate with negative initial energy is shown. We have not discussed the reduction of the GPE to 2d for this case. Also, our simulations do not contain loss terms which become important in condensates at high densities. Thus we do not give a physical interpretation of these results. However, this example shows that the numerical method is applicable to the case of strong focusing nonlinearities in the GPE. Our numerical results confirm that the attractive GPE in 2d with negative initial energy will blow up at finite time (cf. Fig. 9). Furthermore, we point out that the TSSP allows the inclusion of loss terms into the GPE and it is also feasible to solve the GPE in 3d for the attractive case [9]. Therefore the TSSP is a promising candidate for simulating the recent experiments on collapsing and exploding BEC's by Donley et al. [22] which requires full 3d simulations and the inclusion of loss channels.

Example 4 shows the effects of turning on repulsive interactions and changing the trap frequency in a 3d condensate. As expected from our previous simulations we see in Fig. 10 oscillations at twice the trap frequency in directions x, y and z, respectively. The amplitude of the oscillations decreases with increasing frequency, i.e., it becomes more difficult to excite oscillations for larger trap frequencies. This behavior is one of the basic assumptions allowing the reduction of the GPE to 2d and 1d in the cases where one or two of the trap frequencies are much larger than the others (cf. Section 2.3).

The last Example 5 shows the creation of vortices in a 2d BEC by stirring it with a blue detuned laser beam (see also [13,14,41]) where we identify the creation of three vortices in the BEC as shown in Fig. 11. We note that since we study the GPE without taking into account the interaction between the condensate and a thermal cloud of atoms (additional dissipation) no stationary state showing an Abrikosov lattice of vortices is found as in recent experiments [41] and numerical studies on the effects of a thermal cloud [43] on the vortex formation. However, we point out that full 3d simulations including the effects of thermal particles with a very high precision are feasible based on the TSSP.

Finally, we note that the TSSP is a very powerful versatile numerical method for solving the GPE which can be applied to a large number of different physical situations. The efficiency of this method and the high precision of the solutions make the TSSP a good choice for solving experimental situations that are numerically very demanding. Among these we believe that numerical studies of collapsing condensates with attractive interactions and multi-component condensates taking into account all experimentally relevant extensions of the GPE as well as on extensions of the GPE dealing with dissipation mechanisms [28] will be feasible by using the TSSP [9].

5. Summary

We studied a numerical method for solving the time-dependent GPE which describes trapped Bose–Einstein condensates at temperatures T much smaller than the critical condensate temperature T_c. We started with the 3d GPE, scaled it to obtain a four-parameter model, and showed how to approximately reduce it to a 2d GPE and a 1d GPE in certain limits. We provided the approximate ground state solution of the GPE in two extreme regimes: (very) weakly interacting condensates and condensates with strong repulsive interactions. Then, most importantly, we used the time-splitting spectral method in connection with analytical considerations based on perturbation theory (mesh-size control, dimension reduction) to solve the time-dependent GPE in 1d, 2d and 3d. Extensive numerical examples in 1d, 2d and 3d for weakly/

strongly interacting condensates defocusing/focusing nonlinearity, and zero/nonzero initial phase data were presented to demonstrate the power of the time-splitting spectral numerical method. Finally, we want to point out that equations very similar to the GPE are also encountered in nonlinear optics. In the future we plan to apply this powerful numerical method to physically more complex systems like multi component condensates, collapsing condensates with attractive interactions and also to describe coherent atomic samples in wave guides.

Acknowledgements

W.B. acknowledges support by the National University of Singapore Grant No. R-151-000-027-112. P.A.M. acknowledges support from the EU-funded TMR network 'Asymptotic Methods in kinetic Theory', from his WITTGENSTEIN-AWARD 2000 funded by the Austrian National Science Fund FWF, and from Weizhu Bao's grant at NUS. D.J. acknowledges support from the WITTGENSTEIN-AWARD of P. Zoller. This research was supported in part by the International Erwin Schrödinger Institute in Vienna and the START project 'Nonlinear Schrödinger and quantum Boltzmann equations' (FWF Y137-TEC) of N.J. Mauser. The three authors acknowledge discussion with N.J. Mauser and P. Zoller.

References

[1] S.K. Adhikari, Numerical solution of the two-dimensional Gross–Pitaevskii equation for trapped interacting atoms, Phys. Lett. A 265 (2000) 91–96.
[2] S.K. Adhikari, Numerical study of the spherically symmetric Gross–Pitaevskii equation in two space dimensions, Phys. Rev. E 62 (2) (2000) 2937–2944.
[3] A. Aftalion, Q. Du, Vortices in a rotating Bose–Einstein condensate: critical angular velocities and energy diagrams in the Thomas–Fermi regime, Phys. Rev. A 64 (2001) 063603.
[4] G.P. Agrawal, M.J. Potasek, Nonlinear pulse distortion in single-mode optical fibers at the zero-dispersion wavelength, Phys. Rev. A 33 (1986) 1765.
[5] M.H. Anderson, J.R. Ensher, M.R. Matthews, C.E. Wieman, E.A. Cornell, Science 269 (1995) 198–201.
[6] W. Bao, S. Jin, P.A. Markowich, On time-splitting spectral approximations for the Schrödinger equation in the semiclassical regime, J. Comput. Phys. 175 (2002) 487–524.
[7] W. Bao, S. Jin, P.A. Markowich, Numerical study of time-splitting spectral discretizations of nonlinear Schrödinger equations in the semi-classical regimes, SIAM J. Sci. Comput., to appear.
[8] W. Bao, W. Tang, Ground state solution of trapped interacting Bose–Einstein condensate by directly minimizing the energy functional, J. Comput. Phys., to appear.
[9] W. Bao, D. Jaksch, Numerical methods for solving damped nonlinear Schrödinger equations with a focusing nonlinearity, SIAM J. Numer Anal., to appear.
[10] G. Baym, C.J. Pethick, Phys. Rev. Lett. 76 (1996) 6.
[11] C.C. Bradley, C.A. Sackett, R.G. Hulet, Phys. Rev. Lett. 78 (1997) 985.
[12] C. Canuto, M.Y. Hussaini, A. Quarteroni, T.A. Zhang, Spectral Methods in Fluid Dynamics, Springer, New York, 1988.
[13] B.M. Caradoc-Davis, R.J. Ballagh, K. Burnett, Coherent dynamics of vortex formation in trapped Bose–Einstein condensates, Phys. Rev. Lett. 83 (1999) 895.
[14] B.M. Caradoc-Davis, R.J. Ballagh, P.B. Blakie, Three-dimensional vortex dynamics in Bose–Einstein condensates, Phys. Rev. A 62 (2000) 011602.
[15] M.M. Cerimele, M.L. Chiofalo, F. Pistella, S. Succi, M.P. Tosi, Numerical solution of the Gross–Pitaevskii equation using an explicit finite-difference scheme: an application to trapped Bose–Einstein condensates, Phys. Rev. E 62 (1) (2000) 1382–1389.
[16] M.M. Cerimele, F. Pistella, S. Succi, Particle-inspired scheme for the Gross–Pitaevski equation: an application to Bose–Einstein condensation, Comput. Phys. Commun. 129 (2000) 82–90.
[17] M.L. Chiofalo, S. Succi, M.P. Tosi, Ground state of trapped interacting Bose–Einstein condensates by an explicit imaginary-time algorithm, Phys. Rev. E 62 (5) (2000) 7438–7444.

[18] F. Dalfovo, S. Stringari, Phys. Rev. A 53 (1996) 2477;
A.L. Fetter, Phys. Rev. A 53 (1996) 4245;
M. Bayindir, B. Tanatar, Phys. Rev. A 58 (1998) 3134;
B.I. Schneider, D.L. Feder, Phys. Rev. A 59 (1999) 2232.
[19] F. Dalfovo, S. Giorgini, L.P. Pitaevskii, S. Stringari, Rev. Mod. Phys. 71 (1999) 463.
[20] K.B. Davis, M.O. Mewes, M.R. Andrews, N.J. van Druten, D.S. Durfee, D.M. Kurn, W. Ketterle, Phys. Rev. Lett. 75 (1995) 3969.
[21] R.J. Dodd, Approximate solutions of the nonlinear Schrödinger equation for ground and excited states of Bose–Einstein condensates, J. Res. Natl. Inst. Stan. 101 (4) (1996) 545–552.
[22] E.A. Donley, N.R. Claussen, S.L. Cornish, J.L. Roberts, E.A. Cornell, C.E. Wieman, Dynamics of collapsing and exploding Bose–Einstein condensates, Nature (London) 412 (2001) 295.
[23] M. Edwards, P.A. Ruprecht, K. Burnett, R.J. Dodd, C.W. Clark, Phys. Rev. Lett. 77 (1996) 1671;
D.A.W. Hutchinson, E. Zaremba, A. Griffin, Phys. Rev. Lett. 78 (1997) 1842.
[24] M. Edwards, K. Burnett, Numerical solution of the nonlinear Schrödinger equation for small samples of trapped neutral atoms, Phys. Rev. A 51 (2) (1995) 1382–1386.
[25] J.R. Ensher, D.S. Jin, M.R. Mathews, C.E. Wieman, E.A. Cornell, Phys. Rev. Lett. 77 (1996) 4984.
[26] B. Fornberg, T.A. Driscoll, A fast spectral algorithm for nonlinear wave equations with linear dispersion, J. Comput. Phys. 155 (1999) 456.
[27] S.A. Gardiner, D. Jaksch, R. Dum, J.I. Cirac, P. Zoller, Nonlinear matter wave dynamics with a chaotic potential, Phys. Rev. A 62 (2000) 023612.
[28] C.W. Gardiner, J.R. Anglin, T.I.A. Fudge, The stochastic Gross–Pitaevskii equation, J. Phys. B 35 (2002) 1555.
[29] D. Gottlieb, S.A. Orszag, Numerical Analysis of Spectral Methods, Soc. for Industr. & Appl. Math., Philadelphia, 1977.
[30] A. Griffin, D. Snoke, S. Stringaro (Eds.), Bose–Einstein Condensation, Cambridge University Press, New York, 1995.
[31] E.P. Gross, Nuovo. Cimento. 20 (1961) 454.
[32] R.H. Hardin, F.D. Tappert, Applications of the split-step Fourier method to the numerical solution of nonlinear and variable coefficient wave equations, SIAM Rev. Chronicle 15 (1973) 423.
[33] D.S. Jin, J.R. Ensher, M.R. Matthews, C.E. Wieman, E.A. Cornell, Phys. Rev. Lett. 77 (1996) 420.
[34] S. Jin, C.D. Levermore, D.W. McLaughlin, The semiclassical limit of the defocusing nonlinear Schrödinger hierarchy, CPAM 52 (1999) 613–654.
[35] L. Laudau, E. Lifschitz, Quantum Mechanics: Non-Relativistic Theory, Pergamon Press, New York, 1977.
[36] P. Leboeuf, N. Pavloff, Phys. Rev. A 64 (2001) 033602;
V. Dunjko, V. Lorent, M. Olshanii, Phys. Rev. Lett. 86 (2001) 5413.
[37] E.H. Lieb, R. Seiringer, J. Yngvason, Bosons in a trap: a rigorous derivation of the Gross–Pitaevskii energy functional, Phys. Rev. A 61 (2000) 3602.
[38] F.H. Lin, J.X. Xin, On the incompressible fluid limit and the vortex motion law of the nonlinear Schrödinger equation, Commun. Math. Phys. 200 (1999) 249.
[39] P.A. Markowich, P. Pietra, C. Pohl, Numerical approximation of quadratic observables of Schrödinger-type equations in the semi-classical limit, Numer. Math. 81 (1999) 595.
[40] P. Markowich, P. Pietra, C. Pohl, H.P. Stimming, A Wigner-measure analysis of the Dufort0-Fraenkel scheme for the Schrödinger equation, SIAM J. Numer. Anal., to appear.
[41] M.R. Matthews, B.P. Anderson, P.C. Haljan, D.S. Hall, C.E. Wieman, E.A. Cornell, Phys. Rev. Lett. 83 (1999) 2498;
C. Raman, J.R. Abo-Shaeer, J.M. Vogels, K. Xu, W. Ketterle, Phys. Rev. Lett. 87 (2001) 210402;
J.R. Abo-Shaeer, C. Raman, J.M. Vogels, W. Ketterle, Science 292 (2001) 476.
[42] A.S. Parkins, D.F. Walls, Phys. Rep. 303 (1998) 1.
[43] A.A. Penckwitt, R.J. Ballagh, C.W. Gardiner, The nucleation, growth and stabilization of vortex lattices, cond-mat/0205037.
[44] L.P. Pitaevskii, Zh. Eksp. Teor. Fiz. 40 (1961) 646 (Sov. Phys. JETP 13 (1961) 451).
[45] J.L. Roberts, N.R. Claussen, S.L. Cornish, E.A. Donley, E.A. Cornell, C.E. Wieman, Controlled Collapse of a Bose–Einstein Condensate, cond-mat/0102116.
[46] D.S. Rokhsar, Phys. Rev. Lett. 79 (1997) 2164;
R. Dum, J.I. Cirac, M. Lewenstein, P. Zoller, Phys. Rev. Lett. 80 (1998) 2972;
P.O. Fedichev, G.V. Shlyapnikov, Phys. Rev. A 60 (1999) R1779.
[47] P.A. Ruprecht, M.J. Holland, K. Burrett, M. Edwards, Time-dependent solution of the nonlinear Schrödinger equation for Bose-condensed trapped neutral atoms, Phys. Rev. A 51 (6) (1995) 4704–4711.
[48] P.A. Ruprecht, M.J. Holland, K. Burnett, Phys. Rev. A 51 (1995) 4704;
D. Jaksch, S.A. Gardiner, K. Schulze, J.I. Cirac, P. Zoller, Phys. Rev. Lett. 86 (2001) 4733.
[49] B.I. Schneider, D.L. Feder, Numerical approach to the ground and excited states of a Bose–Einstein condensated gas confined in a completely anisotropic trap, Phys. Rev. A 59 (3) (1999).

[50] G. Strang, On the construction and comparison of differential schemes, SIAM J. Numer. Anal. 5 (1968) 506.
[51] T.R. Taha, M.J. Ablowitz, Analytical and numerical aspects of certain nonlinear evolution equations, II. Numerical, nonlinear Schrödinger equation, J. Comput. Phys. 55 (1984) 203.
[52] T.R. Taha, M.J. Ablowitz, Analytical and numerical aspects of certain nonlinear evolution equations, III. Numerical, Korteweg-de Vries equation, J. Comput. Phys. 55 (1984) 231.